Supplemental information

Multimodal microscale mechanical mapping of cancer cells in complex microenvironments

Miloš Nikolić, Giuliano Scarcelli, and Kandice Tanner

Supplementary material

# Multimodal microscale mechanical mapping of cancer cells in complex microenvironments

Miloš Nikolić[1,2], Giuliano Scarcelli[2,3], and Kandice Tanner[1, *]

[1]Laboratory of Cell Biology, Center for Cancer Research, National Cancer Institute, National Institutes of Health, USA

[2]Maryland Biophysics Program, IPST, University of Maryland, College Park, MD, USA

[3]Fischell Department of Bioengineering, University of Maryland, College Park, MD, USA

Effect of the nuclear volume fraction on average Brillouin shift of the whole cell

A)

B)

C)
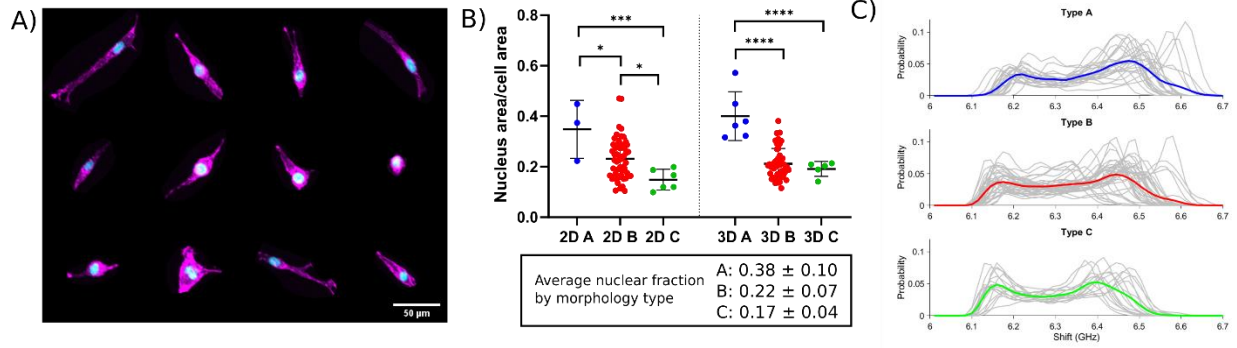
Supplementary Figure 1. Fraction of the nucleus in cell images. (A) Example maximum projection fluorescence images of cells in 2D stained with a nuclear stain (DAPI in cyan) and actin (phalloidin-Atto565 in magenta). The fraction of nucleus is defined as the ratio of the areas of the nucleus and the whole cell which we measured by thresholding the DAPI and phalloidin channels respectively. This analysis was performed in Fiji. (B) Fraction of nucleus in confocal fluorescence images for cells in 2D and 3D conditions. List below is the average nuclear fraction for all cells pooled from both 2D and 3D conditions. (C) Probability distributions of Brillouin shift in all cells from 2D and 3D conditions separated by type. Gray lines indicate individual cells, and colored lines are average distributions.

Supplementary Figure 1 C) shows a heterogeneous mix of individual cells, where the Brillouin shift is distributed with a bimodal distribution per cell. For this dataset, on average the two modes are centered approximately around 6.2 GHz and 6.45 GHz. Previously it has been validated that these two modes correspond to the Brillouin shifts from the cytoplasm and the nucleus respectively (1,2). Assuming that the two modes are Gaussian, the overall mean of the distribution is given by:

$$\mu_{whole\ cell} = f_n\ 6.45\ GHz + (1 - f_n)\ 6.2\ GHz.$$

where f_n is the fraction of voxels inside the nucleus. The difference in the nucleus fraction between type A and type C is about 21% (Supplementary Figure 1 B). Suppose that we measure a theoretical cell with 6.45

GHz shift inside the nucleus and 6.2 GHz inside the cytoplasm, the mean value of the Brillouin shift as a function of f_n is given by:

$$\mu_{whole\ cell} = (0.25\ GHz)f_n\ +\ 6.2\ GHz.$$

In this case the 0.21 change in f_n corresponds to a difference in the mean $\Delta\mu_{whole\ cell} = 52\ MHz$. This is comparable to the measured differences in Brillouin shift across conditions (see Figure 1). It is worth noting that some of the differences in Brillouin shift shown in Figure 3 (e.g. among types within 3D condition) are larger than this value by a factor of 2. This means that not all the differences between different morphology types can be attributed only to the nucleus fraction, although the nucleus plays an important role on the average Brillouin shift of a cell. Therefore, normalizing by multiple relevant parameters is important for understanding the mechanical properties of cells.

**Brillouin microscopy at the cell edge**

Brillouin microscopy is limited when measuring the cell periphery and very thin protrusions. Voxels at the cell edge that straddle the cell boundary can also contain signal from the surrounding media (3-5). In our data we conservatively exclude those pixels (3.5σ away from the mean of the Brillouin shift of the surrounding medium, and manual corrections when necessary. See methods). Supplementary Figure 2 shows the Brillouin shift of cells as a function of the ratio of pixels at the cell boundary to total number of pixels in the cell. As expected from the morphological analysis which shows that elongated and protrusive cells have lower Brillouin shift (see main text), we find a weak correlation (correlation coefficient -0.31) between the perimeter-area ratio and the Brillouin shift. This is expected because the perimeter-area ratio is related to the traditional morphological parameters: circularity and elongation. The poor value of the coefficient of determination ($R^2 = 0.0968$) indicates that for any fraction of the boundary pixels in the cell we observe Brillouin shifts with a large variation that cannot be attributed to the amount of boundary pixels in the images.
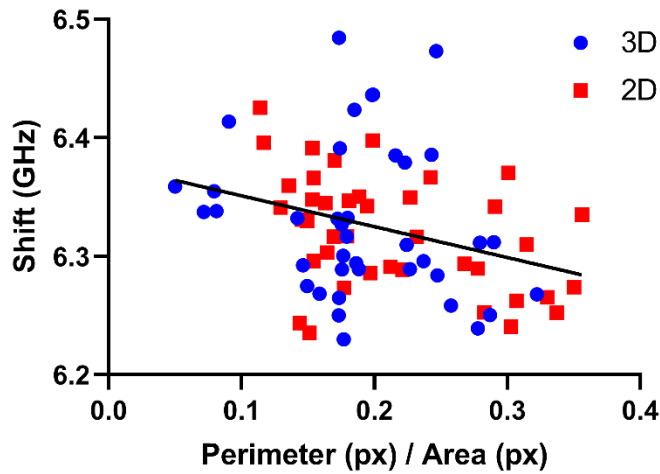
Supplementary Figure 2. Average shift versus the fraction of peripheral pixels in cell image. To confirm that the pixels at the edge of the cell do not affect the overall average shift of the cell, we calculated the fraction of boundary pixels in each Brillouin image. We normalize the number of boundary voxels by the total number of voxels inside the cell used to calculate Brillouin shift (overall cell area in Brillouin map) and plot it against the average Brillouin shift.

Role of cell orientation with respect to the fibrillar topography

Previous work from our lab (6) has shown that cells sense the fibrillar architecture by aligning individual protrusions locally with the fibrillar structure, as well as remodeling the local fibrillar structure. Since cells of type B which have elongated morphology and a preferential axis, also have a higher shift in presence of fibrillar topography (Figure 3. D) we asked if the alignment of the cell axis with the fibrillar architecture correlates with the Brillouin shift of the cell. However, we find no correlation with the Brillouin shift; this could be the result of a poor sensitivity of the measurement due to the high variability of the data especially in thin protrusions or it could suggest that the cells mechanically interact with the fibrillar topography at the level of cell protrusions first, and that the mechanical changes on the level of the whole cell could be downstream effects of that interaction.

FT, type B
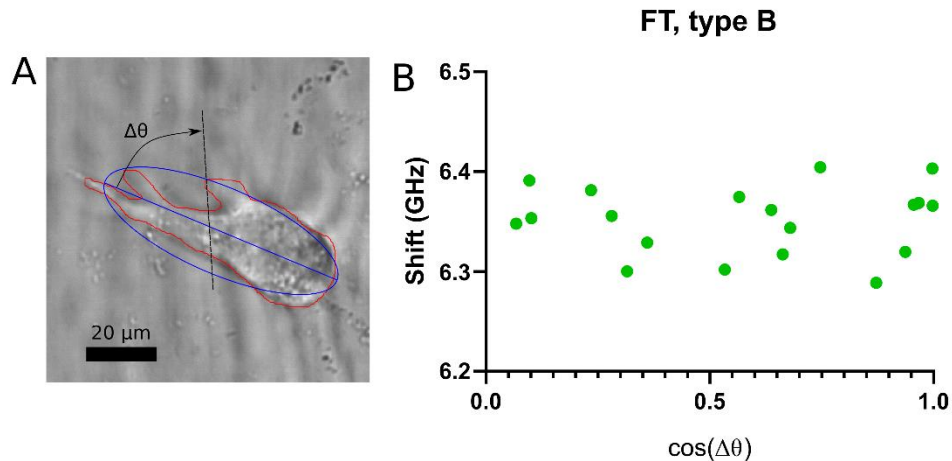
Supplementary Figure 3. Average shift of cell versus alignment with fibrils. (A) Example image of a cell cultured in fibrillar topography. Cell boundary is depicted in red, while the fitted ellipse and the major axis are in blue. The dashed black line is the direction of the local fibrils. Cell alignment is quantified as the cosine of the angle between major axis of the fitted ellipse and the direction of fibrils. (B) Plot of the average Brillouin shift of the cell versus the cell alignment with fibrils. We find no correlation between these two variables (Pearson correlation coefficient = 0.033).

References

1. Zhang, J., F. Alisafaei, M. Nikolić, X. A. Nou, H. Kim, V. B. Shenoy, and G. Scarcelli. 2020. Nuclear Mechanics within Intact Cells Is Regulated by Cytoskeletal Network and Internal Nanostructures. *Small*. n/a(n/a):1907688, doi: 10.1002/smll.201907688, https://doi.org/10.1002/smll.201907688.

2. Zhang, J., X. A. Nou, H. Kim, and G. Scarcelli. 2017. Brillouin flow cytometry for label-free mechanical phenotyping of the nucleus. 17(17), doi: 10.1039/c6lc01443g, http://pubs.rsc.org/en/content/articlepdf/2017/lc/c6lc01443g.

3. Caponi, S., D. Fioretto, and M. Mattarelli. 2020. On the actual spatial resolution of Brillouin Imaging. *Optics Letters*. 45(5):1063-1066, doi: 10.1364/OL.385072, http://opg.optica.org/ol/abstract.cfm?URI=ol-45-5-1063.

4. Caponi, S., D. Fioretto, and M. Mattarelli. 2020. Transition across a sharp interface: Data from Raman and Brillouin imaging spectroscopy. *Data in Brief*. 33:106368, doi: https://doi.org/10.1016/j.dib.2020.106368, https://www.sciencedirect.com/science/article/pii/S2352340920312610.

5. Mattarelli, M., M. Vassalli, and S. Caponi. 2020. Relevant Length Scales in Brillouin Imaging of Biomaterials: The Interplay between Phonons Propagation and Light Focalization. *ACS Photonics*. 7(9):2319-2328, doi: 10.1021/acsphotonics.0c00801, https://doi.org/10.1021/acsphotonics.0c00801.

6. Paul, C. D., A. Hruska, J. R. Staunton, H. A. Burr, K. M. Daly, J. Kim, N. Jiang, and K. Tanner. 2019. Probing cellular response to topography in three dimensions. *Biomaterials*. 197:101-118, doi:

https://doi.org/10.1016/j.biomaterials.2019.01.009,
http://www.sciencedirect.com/science/article/pii/S0142961219300158.